Atmospheric Environment 194 (2018) 58–70

Contents lists available at ScienceDirect

Atmospheric Environment

journal homepage: www.elsevier.com/locate/atmosenv

Use of networks of low cost air quality sensors to quantify air quality in urban settings

Olalekan A.M. Popoola[a,*], David Carruthers[b], Chetan Lad[b], Vivien B. Bright[a], Mohammed I. Mead[a], Marc E.J. Stettler[c], John R. Saffell[d], Roderic L. Jones[a]

[a] Department of Chemistry, University of Cambridge, Lensfield Road, Cambridge, CB2 1EW, UK
[b] Cambridge Environmental Research Consultants Ltd, 3 Kings Parade, Cambridge, CB2 1SJ, UK
[c] Faculty of Engineering, Department of Civil and Environmental Engineering, 614 Skempton Building, South Kensington Campus, Imperial College London, London, SW7 2AZ, UK
[d] Alphasense Ltd., Sensor Technology House, 300 Avenue West, Skyline 120, Great Notley, Essex, CM77 7AA, UK

ARTICLE INFO

Keywords:
Air quality
Low cost sensors
Dense sensor network
Scale separation
Air quality model
Long term measurements

ABSTRACT

Low cost sensors are becoming increasingly available for studying urban air quality. Here we show how such sensors, deployed as a network, provide unprecedented insights into the patterns of pollutant emissions, in this case at London Heathrow Airport (LHR). Measurements from the sensor network were used to unequivocally distinguish airport emissions from long range transport, and then to infer emission indices from the various airport activities. These were used to constrain an air quality model (ADMS-Airport), creating a powerful predictive tool for modelling pollutant concentrations. For nitrogen dioxide (NO_2), the results show that the non-airport component is the dominant fraction (~75%) of annual NO_2 around the airport and that despite a predicted increase in airport related NO_2 with an additional runway, improvements in road traffic fleet emissions are likely to more than offset this increase. This work focusses on London Heathrow Airport, but the sensor network approach we demonstrate has general applicability for a wide range of environmental monitoring studies and air pollution interventions.

1. Introduction

Poor air quality is known to affect human health (Bernstein et al., 2004; Brunekreef and Holgate, 2002; McConnell et al., 2002; Parnia et al., 2002; Pope and Dockery, 2006; Ren et al., 2017; Samoli et al., 2008; WHO, 2009). Urban air quality monitoring, traditionally the remit of expensive and complex reference instruments (Kumar et al., 2015; National Audit Office, 2009) can now be achieved using readily deployable low cost instruments, revolutionising approaches to the study of urban pollution. Over the last few years, low cost sensors have been assessed for their viability in monitoring ambient air quality including measurements of gaseous and particulate matter (PM) pollutants. Whilst some studies show that there are still some challenges with using off the shelf devices (Borrego et al., 2016; Lewis et al., 2016), other studies have demonstrated that some of these limitations can be overcome with careful data processing and network design (Crilley et al., 2018; Kim et al., 2018; Penza et al., 2014; Popoola et al., 2013; Sun et al., 2017; Spinelle et al., 2015; De Vito et al., 2018; Heimann et al., 2015). There have also been attempts at deploying portable sensors as networks to better understand the spatial variability of air pollution (Mead et al., 2013; Miskell et al., 2017; Mueller et al., 2017; Penza et al., 2014; Sun et al., 2016). Schneider et al., 2017 also used a data fusion technique to combine sensor network data with an air quality model which was then used to simulate the spatial pattern of pollutants.

Although there have been several studies on the impact of aviation on ambient air quality (Carslaw et al., 2006; Herndon et al., 2004, 2008; Hu et al., 2009; Masiol and Harrison, 2015; Schürmann et al., 2007), they mainly focused on using sparse array of fixed stations or short term mobile platforms which allowed source apportionment studies within and in the proximity of the airports.

Here we show how low cost air quality instruments, when deployed as a network rather than as individual sensors, provide unprecedented additional insights into the patterns and sources of air pollution.

The case study we have applied this methodology to is London Heathrow Airport and focusses in this paper mainly on NO_x. The limit value for annual average NO_2 of 40 μg/m^3 is not currently being met at some of the areas around London Heathrow airport. The expansion of

* Corresponding author.
E-mail address: oamp2@cam.ac.uk (O.A.M. Popoola).

https://doi.org/10.1016/j.atmosenv.2018.09.030
Received 1 February 2018; Received in revised form 12 September 2018; Accepted 17 September 2018
Available online 18 September 2018

the airport, including a third runway (UK Department for Transport, 2017), has raised concerns that meeting this limit value would be unachievable in the future. The sensor network we deployed at the airport consisted of up to 40 nodes sited across the airport and covering a range of emission environments, each measured a range of species including NO_2, NO, CO and CO_2. The sensor network, together with the novel analysis approach we describe, has allowed pollutant emissions attributable solely to the airport activities to be distinguished from other non-airport related sources. Using the CO_2 measurements made across the network this, in turn, has allowed the direct quantification of NO_X and CO emission indices for a number of different airport related activities.

These measurements, and in particular the direct determination of emission indices, were used to optimize the ADMS-Airport air quality model, creating a powerful predictive tool for pollutant concentrations in and around Heathrow airport.

While this study focuses on the UK's Heathrow Airport, the techniques we describe, that exploit the emerging low-cost air quality sensor technologies and novel analysis approaches, have far wider applicability for environmental monitoring and air pollution interventions.

2. Materials and methods

In this section we briefly describe the low cost sensor network used for the study at LHR, including the state-of-the art modelling air quality model utilised in our study.

2.1. Sensor measurement: SNAQ boxes and network deployment

The sensor nodes were low cost portable air quality devices developed at the Department of Chemistry, the University of Cambridge, UK, as part of NERC (Natural Environmental Research Council) funded Sensor Network for Air Quality (SNAQ) project at London Heathrow airport. Each node measured the parameters summarised in Table 1, made at a 20 s time resolution. In addition, each node was equipped with GPRS and GPS for near real-time data transmission and location/time data respectively (Popoola et al., 2013). Both the particle size and gas species devices were calibrated under laboratory conditions, with the ambient performance of the NO, NO_2 and the CO_2 sensors presented in section 2.2.

Although a network of 40 sensor nodes was ultimately deployed, we are focussing here on a five-week period (4 October-11 November 2012) where only 17 of the sensor network nodes were fully operational, but where additional information on aircraft throttle settings was available (Fig. 1). The sensor network was designed to cover, as far as possible, the different activity zones in and around the airport including the terminals, runways and the main airside roads (Fig. 1). To contextualise the network density, only one routine air quality reference station (LHR2) is located within the deployment zone, with node S47 co-located with this reference station. Two nodes (S47 and S48) were also sited close to each other (~5 m apart), and, were used to study the reproducibility of the SNAQ measurements. All the nodes were mounted at 3 m on lampposts within the airport perimeter. Fig. 2 (and Fig S1) illustrate the high temporal and spatial variability within the airport, influenced by both airport and non-airport related emissions captured by the network.

Table 1
Species measured and techniques for the sensor nodes used for the SNAQ Heathrow study. Only those sensors shown in bold are used in this study.

Species	Methodology	Description of sensor
CO	**Electrochemical**	**Alphasense B4**
NO		
[a]NO_2		
CO_2	**Non-Dispersive Infra-Red**	**Sensair K33**
VOCs (total)	Photo Ionisation Detector	Alphasense PID-AH
Temperature	Pt Resistance Sensor	Pt1000
Relative Humidity	Polymer Capacitive Element	Honeywell HIH4000
Wind Speed/Direction	**Sonic Anemometer**	**Gill WindSonic**
Size Speciated Particulates (ranging 0.38–17.4 μm)	Optical Particle Counter	University of Hertfordshire

[a] The NO_2 sensors used here were 100% cross sensitive to O_3. The data was corrected for this cross interference (see section 2.2), and where it is not the species is presented as O_X (i.e. NO_2 + O_3).

2.2. Sensor measurement validation

The performance of the SNAQ units for NO and NO_2 was evaluated by comparing the results from the node co-located with the reference air quality site within the airport (LHR2). Hourly averaged NO_2 data were derived from the hourly O_X reading by correcting for O_3 interference using hourly modelled O_3 data. Comparison of the standard measured gas species (e.g. NO_X) showed that the SNAQ measurements captured variations at the airport with good agreement indicated by the slope (0.9379 ± 0.0081) and coefficient of determination $R^2 \approx 0.95$ (Fig. 3A). This comparison was performed by taking hourly averages of the high temporal resolution (20 s) sensor measurements as the reference data were only reported as hourly averages. As there was no local CO_2 reference instrument available, validation of the SNAQ CO_2 measurements was performed post-study by comparing CO_2 observations made after the deployment with those of a Picarro G2201-I CO_2/CH_4 analyser (Fig. 3B), giving results with a slope of (0.9553 ± 0.0021) and coefficient of determination $R^2 \approx 0.92$. Although, this validation was performed using a single sensor node, we have demonstrated in this study - as with previous studies (Popoola et al., 2016; Mead et al., 2013) - the high level of sensor-sensor repeatability (slopes between 0.9 and 1.0 for all gas species), in this case for two nodes (S47 and S48) which were near co-located for the measurement period (Fig. 4). Errors are standard errors of the ordinary least square estimates.

2.3. Source apportionment

This section describes how we estimate the network baseline (referred to as the non-local signature) which is due to non-local emissions for the measurement period presented in this work (4 October to 11 November 2012).

The major novelty of the sensor network work described here is that local (airport) and non-local (non-local/airport related) fractions of the measured species could be determined independent of wind conditions directly from the network observations without the need for long-term (years) measurements, conditions that limit the extraction of similar information from the traditional sparse routine network measurements. We extracted both the airport fraction and non-airport fraction, as described below, using the local signature to validate the source apportionment of a model, the ADMS-Airport.

Measurements at each sensor node within the network comprise a contribution attributable to emissions local to that sensor – the local signal, and a component advected from outside the network area which will be essentially identical at all sites – the non-local signal.

As emissions of NOx and CO local to each site will always lead to locally elevated concentrations of the pollutants, the concept is then to establish the minimum value of each pollutant across the entire network within a given time window and to equate that to the baseline or non-local signal for that species and period.

To illustrate the process, we will consider for simplicity a three-sensor sub-network with measurements from three nodes (site29, site50 and site19 designated S_1, S_2 and S_3 respectively). In this (arbitrarily chosen) period, S_1 is located at a high pollution site, while S_2 and S_3 are

Fig. 1. Instrumentation and deployment: (A) A typical SNAQ sensor node showing the main components, (B) A Google map © showing the location of London Heathrow airport relative to Central London, UK, and (C) the locations (red tags) of the sensor nodes during the study period and the reference monitoring station LHR2 (blue tag) relative to the terminals (1, 3, 4 and 5, all in purple). (For interpretation of the references to colour in this figure legend, the reader is referred to the Web version of this article.)

located at low pollution sites. The data at 20 s resolution, for three hours only in this illustration, are actual measurements used in this study and are shown in Fig. 5 (red, blue, green).

It can be immediately seen that site S_1 has highly variable CO values, significantly elevated above any hemispheric background value (200–300 ppbv) (Lowry et al., 2016). In contrast, sites S_2 and S_3 both show lower variability, and lower absolute CO values. While sites S_2 and S_3 do both show some isolated pollution events, they together define a clear baseline, which in this period is around 400 ppbv and shows a slight upward trend over the three hour period. Fig. 5B, shows a probability histogram for a single hour of the ensemble of measurements shown in Fig. 5A. A clear maximum in probability is seen at ~400 ppbv, associated with measurements from the low pollution sites where the baseline dominates across this sub-network. This reflects the low CO values associated with predominantly the absence of pollution events at sites S_2 and S_3, while site S_1 mainly contributes to the less frequent but more elevated CO values (> 1000 ppbv). The baseline for this period is extracted by taking a percentile (in this case the 10th) of the measurements from the network (in this case just from the three sites) for the defined period, typically one hour. A percentile is chosen rather than the minimum to account for the measurement error for the sensors, with the choice of the 10th percentile reflecting the typical sensor error. The difference between the minimum CO value measured and the 10th percentile in this case is < 10 ppbv (see expanded probability histogram). These differences, which are broadly representative of the entire dataset for CO, are negligible compared to the pollution levels observed (see e.g. Fig. 6). The baseline shown in Fig. 5A is constructed from a linear interpolation between the baselines obtained for individual hour of data (and an additional hour before and after) and, as can be seen, reproduces both the average baseline and trend. A similar approach (Fig. S2) is applied to the other species (except for NO_2, where hourly O_3 corrected data (see section 2 above) was used with the time window of three hours instead of one hour used for the 20 s resolution data). Although three sensors were used in this illustration, the entire network (17 sensor nodes) were used in the baseline determinations presented below.

Applying the above method to the sensor data for each gas species, we successfully extract the network baseline and use this to determine the local signal (Fig. 6 shows results of the source attribution methodology for CO, and Fig. S3-S4 shows results for CO_2 and NO_2).

2.4. Modelling approach

The model used in this work is ADMS-Airport. This model is an

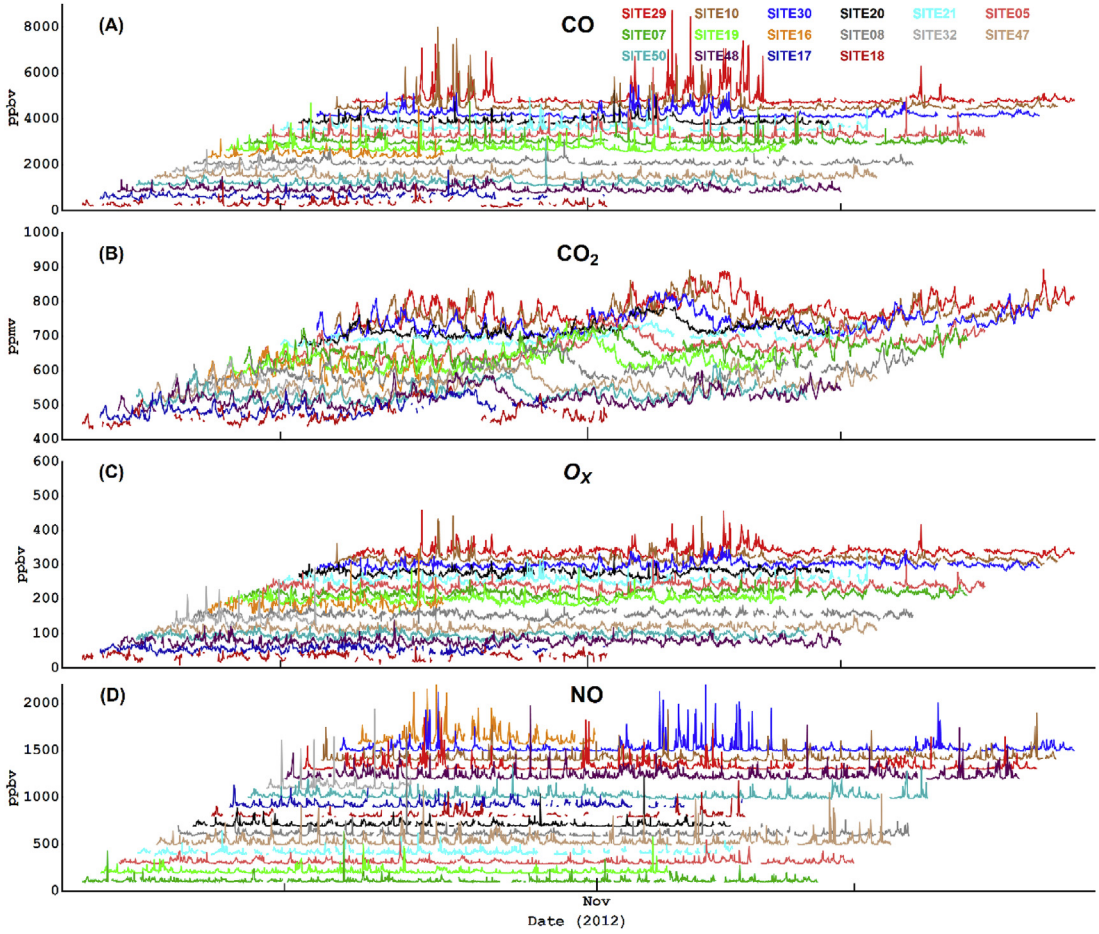

Fig. 2. Time series plots of measurements for the entire five-week study period. From top to bottom are (A) carbon monoxide, (B) carbon dioxide, CO_2, (C) the sum of NO_2 and O_3 (O_X), and (D) nitric oxide, NO.

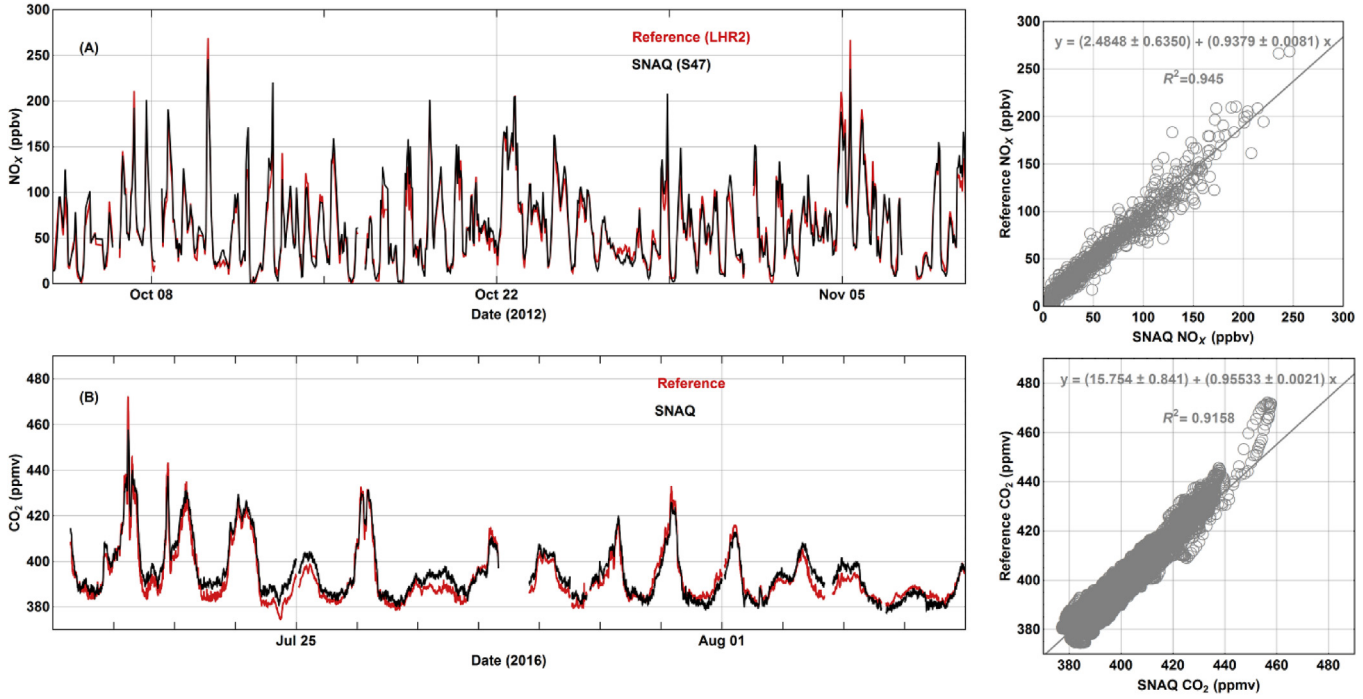

Fig. 3. Comparison between reference method and SNAQ. Temporal variation plots (left panels), and scatter plots (right panels). (A) Hourly average NO_X comparison at LHR2. (B) Minute average CO_2 comparison. Note there are no comparisons for CO and CO_2 at LHR2 as these species are not part of the species routinely monitored at the reference station. The occasional missing data are due to data transmission issues.

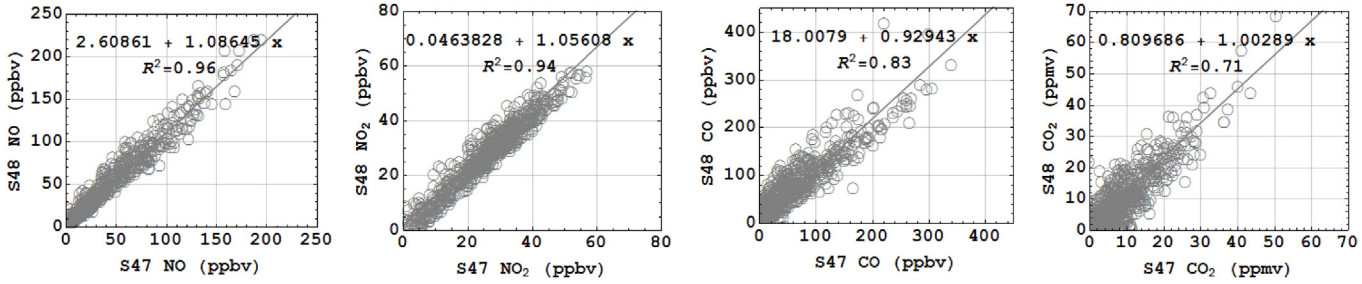

Fig. 4. Correlation plots for SNAQ data for sites 47 and 48. From left to right, hourly mean absolute NO, NO_2, local CO and CO_2.

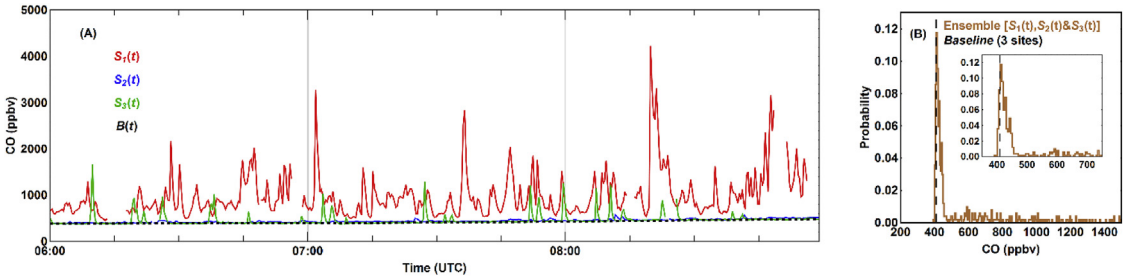

Fig. 5. Time series and probability histogram plot for CO data. (A) time series at 20 s resolution for a three-hour period at three sites in the network (red, green, blue) along with the fitted baseline (dashed black). (B) probability histogram of the combined measurements for the last hour (08:00–09:00) of the three-hour period, with the inset figure showing the same probability histogram on an expanded scale. The 10th percentile of the data is shown in both figures (black dashed). See text for further details. The occasional missing data are due to data transmission issues. For clarity, we have not shown the whole mixing ratio range for both the main and inset images in Fig. 5B. (For interpretation of the references to colour in this figure legend, the reader is referred to the Web version of this article.)

extension of the street scale resolution ADMS-Urban dispersion model (McHugh et al., 1997) for complex urban environments with additional capability for the explicit modelling of aircraft jet engine emissions as jet sources. ADMS-Airport has been recommended by the Project for the Sustainable Development of Heathrow (PSDH) used at Heathrow Airport (UK Department for Transport, 2006) and has been used by the Airports Commission (Module 6 (2015)) as well as the proponents of the three airport expansion schemes considered by the Airports Commission. The overall approach has been to set up an optimised modelling system for a base year of 2012 making extensive use of the sensors, and then to project the airport impact forward to 2030. Model and inventory optimisation for the airport sources was based on the detailed analysis of local fractions of model and monitored data for the sensor locations site 29 and site 30, located north and south of the 09R runway (Fig. 7). Details of model configuration for the hourly and annual predictions are described below.

2.4.1. Hourly average model simulation

Airport emissions were based on a 2012 airport inventory complied by AEA Environment and Energy (AEA, Energy and Environment, 2010) which was then refined using emissions calculated from detailed aircraft activity data for the two-week period 4th November 2012 to 18th November 2012, provided by Heathrow Airport Limited from the Business Objective Search System (BOSS) database, together with CERC's Aircraft Emissions Calculator. This combines European Civil Aviation Conference Report on Standard Method of Computing Noise Contours around Civil Airports performance model (European Civil Aviation Conference, 2005) with Boeing Fuel Flow Method 2 (Doc 9889, 2011). The spatial elements for aircraft emissions and details for all other airside emissions i.e. ground support equipment and auxiliary

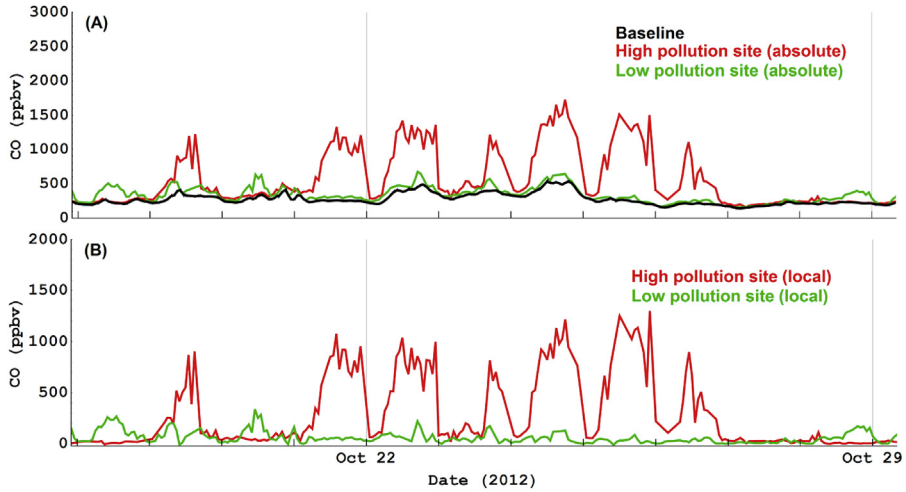

Fig. 6. Time series plot from 18–28 October 2012 for hourly averaged absolute, baseline and local CO data at two sites. (A) Network baseline relative to the absolute mixing ratios, (B) the extracted local mixing ratios.

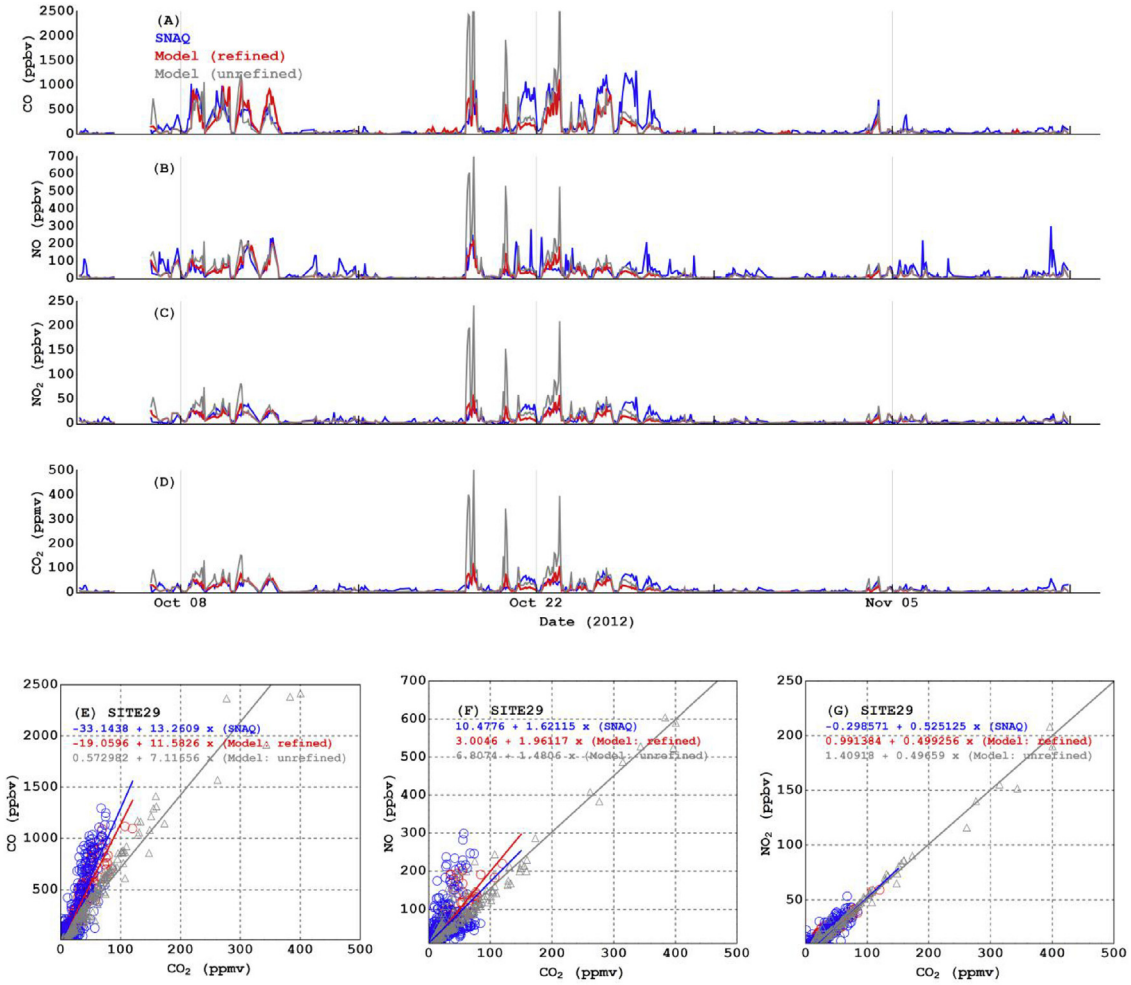

Fig. 7. Comparison of measurement and ADMS model runs. (A–D) time series of CO, NO, NO_2 and CO_2. (E–G) scatter plots of modelled airport CO and NO_2 concentrations (ppbv) against modelled airport CO_2 concentrations (ppmv) for Site 29 sensor location (unrefined model in grey, improved model in red). (For interpretation of the references to colour in this figure legend, the reader is referred to the Web version of this article.)

power units were also obtained from the AEA inventory.

Based on these data the following model/emission improvements were made:

- The dimensions of stand sources were modified to be more representative of the area of emissions;
- The location of take-off sources on runway 09R were moved to better represent the actual start of take-off roll points. For consistency with the new take-off locations, 09R taxi-out and initial climb sources were also moved.
- The treatment of taxiing was refined as follows:
  - a default aircraft speed of 15.4 m/s was previously used for taxiing. There is relatively low model sensitivity to taxiing speeds, but to ensure greater consistency with actual aircraft operations, a speed of 5 m/s was adopted for shorter taxi segments of less than 300 m in length.
  - In addition to engine emissions from the Landing and Take-off (LTO) cycle, taxiing emissions were also modelled as jet sources taking account of the momentum and buoyancy of the source, rather than as ground level volume sources with no initial momentum or buoyancy.
- NO_X and CO taxiing emissions indices were recalculated assuming thrust levels of 4% for short taxi segments and 6.5% for longer segments, together with emission factors for NO and CO which were derived from measured concentration ratios with CO_2 from the sensor network data, rather than the ICAO (International Civil Aviation Organization) default emission factors for 7% thrust. When compared to the ICAO default thrust level of 7% for taxiing, these reduced thrust levels lead to higher CO emission indices and lower NO_x emission indices.

Fig. 7 shows scatter plots of the modelled airport contribution to CO, NO and NO_2 concentrations (ppbv) against the contribution to CO_2 concentrations (ppmv) at the site 29 sensor location, before and after the model refinements. The plots highlight the following effects of the refinements: the large reduction in modelled near ground level concentrations due to the replacement of passive volume sources with buoyant jet sources from taxiing emissions which results in significant plume rise; an increase in the average CO/CO_2 ratios and an increase in the average but greater spread of the $NO_x(NO + NO_2)/CO_2$ ratios, due to the higher CO emission indices and lower NO_x emission ratios, used for the lower thrust settings for taxing, and the increased relative contribution of take-off NO_x emissions to taxiing NO_x emissions at the site.

2.4.2. Annual average model simulation

Non-airport emissions were obtained from the London Atmospheric Emissions Inventory (LAEI) and Slough Emissions Inventory (SEI). 2012 inventories projected from 2008 base year inventories were used; these were the latest versions of the LAEI and SEI available for the study. The road traffic emission factors used to compile these versions of the LAEI and SEI were found to underestimate real world emissions from diesel

vehicles, therefore road emissions were recalculated using modified emission factors for Euro 2 to Euro 5 diesel vehicles. Non-airport emissions within 10 km of the airport were included within the model. Major roads and large industrial sources within 7 km of the airport were modelled explicitly, with all other non-airport emissions modelled as an aggregated source on a 1 km^2 basis.

Monitored concentrations from rural and suburban sites in the Defra's AURN network and the London Air Quality Network (LAQN) were used to estimate the background concentrations due to sources more than 10 km from the airport. Wind-direction dependent background concentrations for the modelled area were calculated using hourly concentrations from Harwell, Southall and Barnes Wetlands monitoring sites. This model set-up allowed use of the Generic Reaction Set chemistry scheme (Venkatram et al., 1994), considering NO_x chemical reactions on an hour-by-hour basis.

Hourly sequential meteorological data from Heathrow Airport was used as input to the model. A surface roughness value of 0.2 m was used for the meteorological measurement site and a value of 0.5 m for the modelling domain (Air Quality Studies for Heathrow, 2007).

Apportionment of the contribution of airport and non-airport emissions to concentrations of NO_x and NO_2 was also carried out. Included within airport emissions is the contribution from all airside emissions and the airport related traffic on surrounding major roads. It is assumed that all traffic on the airport perimeter road along with M4 and M25 spur roads, leading to the airport, is airport related traffic. The traffic flows on these roads is used to apportion an airport traffic contribution on adjacent major roads. To calculate the airport contribution to NO_2 the difference between two model runs was determined: the first including all emissions, the second excluding airport emissions.

The model performance was also verified against Defra and local authority automatic monitors around the airport in 2012, the results showed excellent agreement between modelled and monitored concentrations as summarised Table 2.

2.4.3. Year 2030 and third runway scenarios

The modelling for 2030 considered aircraft fleet changes and airport activity changes, with and without a third runway at Heathrow, equivalent to the 2030 North-West Runway (three runways) and 2030 Do-minimum (two runways) scenarios in the Airports Commission modelling. In addition, a 2012 North-West Runway scenario was modelled i.e. a third runway at Heathrow with the current aircraft emissions technology. Only the airside emissions were modelled for these scenarios due to the uncertainty in road layout with the extended airport.

Scenario aircraft emissions for 2030 were calculated by scaling the 2012 emissions by aircraft movements and fleet-weighted NO_x emissions by aircraft category for 2030 used in the Airports Commission modelling. The location of the new runway and associated taxiways and stands are based on submissions by the scheme proposer to the Airports Commission (Independent report, 2014). Stand emissions are calculated by scaling the baseline 2012 emissions by annual passenger projections.

Runway activity assumed the ending of the Cranford Agreement (LHR Airports Limited, 2016).[1] The scheme design with the third runway proposes rotating runway use between, four modes of operation based on the northern and southern runways alternating between mixed and segregated mode operation, and the central runway operating in segregated mode only. For the modelling, it is assumed that there is, equal use of the four modes during the year, weekly alternation between departure and landing operation on the central runway and intra-day switch between mixed-mode and segregated mode operations on the northern and southern runways.

The airport contribution to total annual average NO_2 concentrations was calculated from modelled annual average NO_x concentrations using primary NO_2 dependent NO_x:NO_2 correlations based on the 2012 baseline modelling including airport and non-airport emissions and using the ADMS chemistry scheme. This was necessary since only sources of NO_x related to the airport were modelled for 2030, which meant that the chemistry scheme within ADMS could not be employed for the 2030 calculations. These NO_2 concentrations, calculated from model derived NO_x:NO_2 correlations, were found to be broadly similar to concentrations obtained using Defra's NO_x to NO_2 Calculator tool (Department for Environment, Food and Rural Affairs, 2016; Jenkin, 2004) for deriving NO_2 concentrations from road NO_x contributions when the primary fraction of NO_2 emissions was typical of road traffic emissions.

Table 2
Comparison of monitored (Mon) and modelled (Mod) 2012 annual average concentrations (μg/m^3).

Location	NO_x (μg/m^3)		NO_2 (μg/m^3)		O_3 (μg/m^3)	
	Mon	Mod	Mon	Mod	Mon	Mod
LHR2	106	104.0	48	50.8	–	30.3
Harlington	61	58.7	35	37.1	34	37.5
Heathrow Green Gates	63	60.1	33	36.1	–	39.8
Heathrow Oaks Road	52	53.8	30	31.6	–	42.0

2.4.4. Emission Factor Toolkit (EFT) version 7.0 road traffic NO_x emissions

NO_x emissions by vehicle type from Defra's EFT v7.0 are shown in Table 3 for the average traffic speed on Bath Road (37 km/h), along with total emissions for the typical traffic flow on the road; a decrease of over 80% in NO_x emissions between 2013 and 2030 can be seen. The EFT v7.0 includes emissions factors extracted from COPERT 4 v 11.0; an update of the EFT taking into account revised emission factors for the majority of Euro 5 and Euro 6 light duty diesel vehicles in COPERT 4 v 11.4 is expected to be released by Defra shortly. Emissions of light duty petrol vehicles and all heavy duty vehicles are unchanged between COPERT 4 v 11.0 and COPERT 4 v 11.4. The emissions for all Euro 6 light duty diesel vehicles in EFT 7.0 have emission limit conformity factors in the range 2.6–2.8 (0.208 g/km to 0.224 g/km compared to the type approval limit of 0.08 g/km at 33.6 km/h, in accordance with Defra's definition of conformity factors). The updated emissions in COPERT 4 v 11.4 take into account the legislative stages of the Euro 6 standard, with the introduction of Real Driving Emissions (RDE) regulations from 2017 (Euro 6c and Euro 6d); for 2017–2019 vehicles (Euro 6c), the updated emissions have conformity factors in the range 3.94–5.05 (0.315 g/km to 0.404 g/km) and for post-2020 vehicles (Euro 6d) conformity factors in the range 1.97–2.45 (0.158 g/km to 0.196 g/km); this is expected to lead to a reduction in road transport emissions along Bath Road for 2030 when compared with emissions calculated using COPERT 4 v 11.0 (Updated Air Quality Re-analysis, 2017).

3. Results

3.1. Air quality network measurements

To illustrate the type of information available using the low cost sensor technique, Fig. 8 shows time series of 20 s average carbon monoxide (CO) across the network on varying timescales: for the entire period in this study, for a week and for a single day. For clarity, the data are ordered from low to highly polluted sites in each panel. Several of the sensors have incomplete time series because of power supply and data transmission issues, however an overall pattern is clear. Firstly, there is a diurnal periodicity evident, with some sensor locations, generally those close to direct aircraft emissions (e.g. S10, S29, S30), showing high levels of CO in contrast to other locations at which much

[1] http://www.heathrow.com/noise/heathrow-operations/cranford-agreement#, accessed 3rd November 2016.

Table 3
EFT 7.0 NO_x emission factors by vehicle type (g/km) and total emissions for Bath Road traffic flow (g/km/s), 2013 and 2030 fleet assumptions.

NOx emission factors at 37 km/h (g/km/vehicle)	2013	2030	Emissions reduction 2013 to 2030	EFT fleet assumptions for 2030 (for road type: Outer London Urban)
Petrol Cars (includes hybrids)	0.182	0.048	73.5%	97% Euro 6
Diesel Cars (includes hybrids)	0.624	0.233	62.6%	95% Euro 6
Taxis	0.868	0.052	94.0%	11% Euro 6; 87% zero emission vehicles
Petrol LGVs	0.009	0.004	56.9%	86% Euro 6
Diesel LGVs	0.749	0.209	72.1%	98% Euro 6
Rigid HGVs	3.846	0.316	91.8%	99% Euro VI
Artic HGVs	6.360	0.422	93.4%	98% Euro VI
Buses/Coaches (includes hybrids)	5.511	0.319	94.2%	> 98% Euro VI
Motorcycles	0.119	0.037	69.1%	> 70% Euro 5 (highest motorcycle standard)
NOx emissions (g/km/s) for Bath Road traffic	**2013**	**2030**	**Emissions reduction 2013 to 2030**	**Traffic breakdown**
All vehicles (32,989 vehicles/day)	0.296	0.051	82.7%	76.4% cars; 8.7% taxis; 6.4% LGVs; 5.2% Buses & coaches; 2.0% Rigid HGVs; 0.4% Articulated HGVs; 1.0% Motorcycles

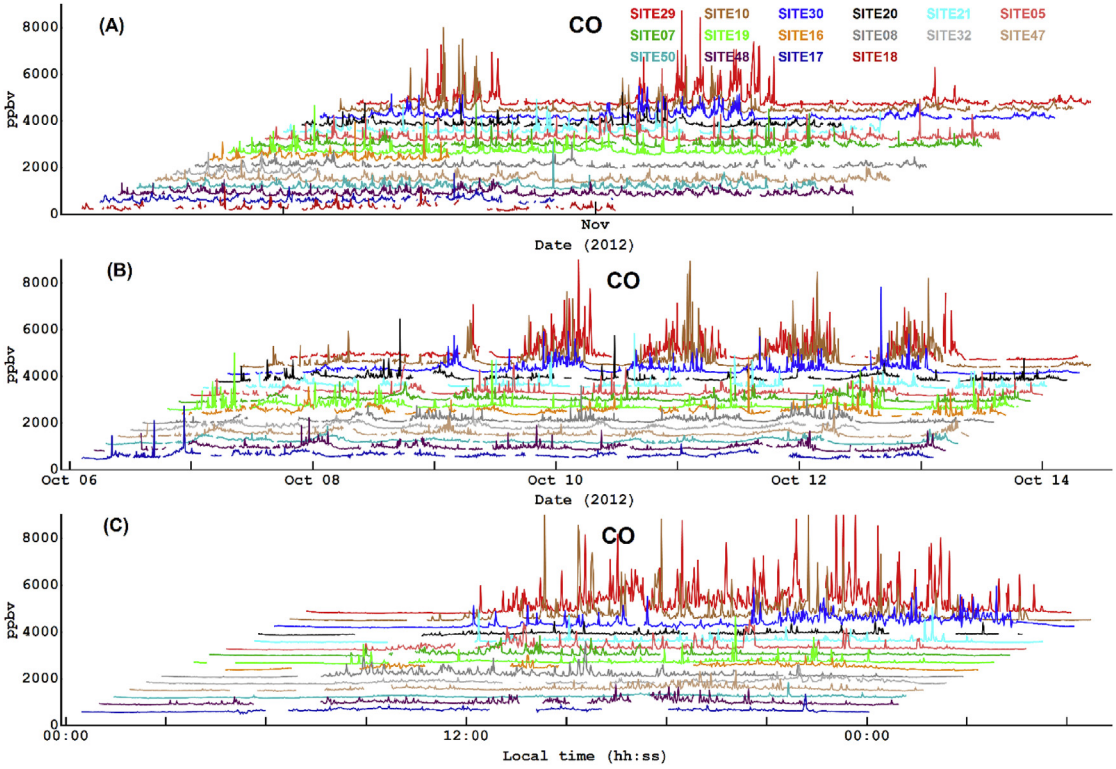

Fig. 8. Time series plots of carbon monoxide measurements across the network nodes operating during the study period: five-week study period (A), one week (6–12 October 2012 - B) and the one day (8 October 2012 -C). Equivalent plots for other species are shown in Fig. S2.

lower levels are seen (e.g. S17, S48). For the overall data set (Fig. 8A), the coarse pattern is that there are two periods of several days of highly polluted conditions separated by less polluted periods. These differences are associated with changing general meteorological conditions, mainly wind direction, which influences runway usage (direction of take-off) and background pollutant concentrations as well as the dispersion of pollutants. Viewing a week of data (Fig. 8B) the strong diurnal pattern associated with the daily airport operation becomes clearer, and finally, looking at a single day (Fig. 8C), individual pollution events can be seen associated with single aircraft movements. Similar patterns are observed across the network for the other species (see Fig. 2).

The main novelty of this deployment was that there were multiple sensors positioned as components of a network of sensor nodes across the airport. Individual sensors in the network measure pollutant levels which are a combination of emissions local to that site and those from further afield. The critical point is that while individual sensors have pollutant signatures unique to the emission sources close to each site, sources which are external to the network itself (as a whole) produce a near identical response across every node of the network. The methods used to distinguish individual sensor responses (local signatures) from the network signature (non-local signature) are presented in section 2.3. The method was applied to all the sensor nodes in the network, and examples of such a separation for NO_2 and CO_2 are shown for a single site (S29) in Fig. 9.

For both NO_2 and CO_2 the observations at this site (which we term absolute) show periods of significant diurnal variation (in excess of 50 ppmv and 50 ppbv for CO_2 and NO_2 respectively), interspersed with periods where diurnal patterns are less evident. In contrast, the network measurements (which we term non-local or baseline) show less diurnal variation but do show longer periods of elevated pollutant concentrations, for example around October 9th and October 24th. Both types of

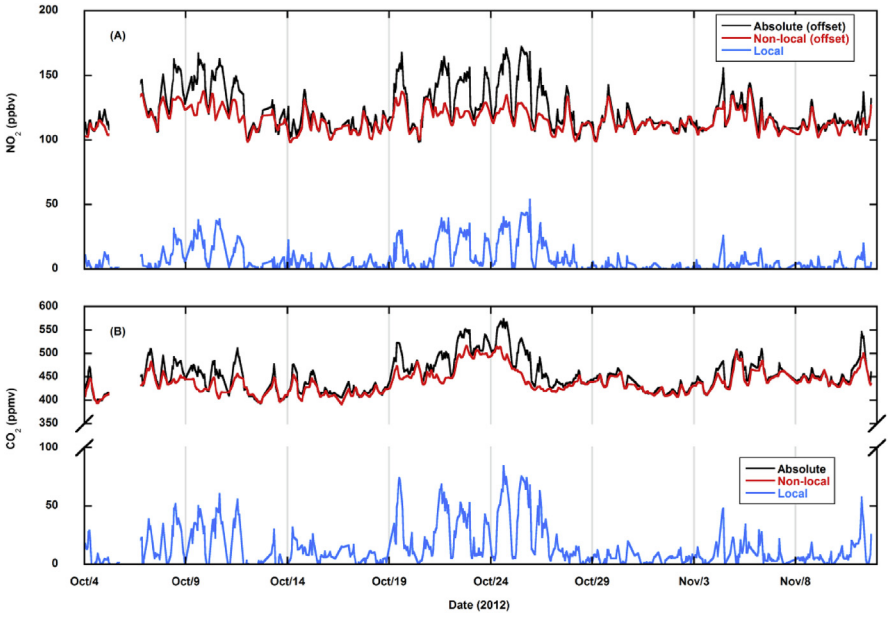

Fig. 9. Time series depicting elements of the source separation for site 29 over the five-week study period. The upper panel (A) observed (absolute) values, together with local and non-local signatures (see text for definitions) for NO_2 and with the equivalent plot for CO_2 (B). Observations obtained at the site are shown in black (with offset of 100 ppbv for absolute and non-local NO_2 applied for clarity), with the network (non-local) signature in red. The derived local measurements are shown in each case in blue. (For interpretation of the references to colour in this figure legend, the reader is referred to the Web version of this article.)

features are characteristic of meteorological impacts on dispersion of pollutants, runway usage, and, as will be seen below, longer range transport of pollutants. Finally, for both CO_2 and NO_2 the site specific (local) signatures retain the diurnal patterns, with the underlying longer-term variations removed.

Polar bivariate plots (Carslaw and Ropkins, 2012), where pollutant concentrations for a time series are shown as functions of wind speed and wind direction, are powerful tools for source attribution studies, both for source location and for providing the basis for the determination of emission indices. Fig. 10A–D shows polar bivariate plots for the hourly average local signatures (i.e. absolute measurements with the network baseline signature removed) for CO, NO, NO_2 and CO_2 for the site discussed above (site 29). The meteorological data (wind speed and direction) for these analyses are taken from the anemometer on the sensor node itself (see panel (E)). The main features in Fig. 10A–D are two distinct regions of elevated concentrations to the NE and SE of the measurement site, both associated with aircraft activities near site 29. The NE lobe shows lower levels of both NO_x ($NO + NO_2$) and the ratio of NO_x to CO_2 and higher levels of CO than the SE lobe, signifying aircraft taxiing to the NE and aircraft taking off to the SE. This is consistent with the location of a taxiway and the runway relative to site 29 (Fig. 1C). NO_2 is comparable for both lobes, consistent with the lower NO but much higher ratio of NO_2 to NO_x for taxiing emissions than for take-off emissions (Herndon et al., 2004). CO_2 in the NE lobe is also higher than in the SE lobe, which considering that the emissions rate of CO_2 is higher for take-off, suggests poorer initial dispersion of taxiing emissions relative to take-off emissions. The figures thus illustrate the additional benefits of multi-species measurements in characterising sources in detail as well as combining them with meteorological information. Note also that the higher concentrations in the local measurements are generally associated with higher wind speeds from the source direction reflecting the buoyant nature of ground level aircraft jet engine plumes (Bennett et al., 2010).

As is discussed in section 2.3, once the local pollutant signatures for each node are obtained (i.e. the background signature removed), emission indices (the amount of pollutant emitted per unit of CO_2) can now be calculated for the different sites. Fig. 4 shows how concentrations of local NO, NO_2 and CO vary with the local CO_2 at site 29. The ratio of the measurements (the graph gradient) is then used to estimate the emissions index (Table S1) for that pollutant which, in this case, correspond to 26.7 ± 0.56 g/kg for CO, 3.50 ± 0.16 g/kg for NO_2, and 1.70 ± 0.04 g/kg for NO. Note that as these are ratios of co-emitting species, they are not dependent on the degree to which any plume is intersected.

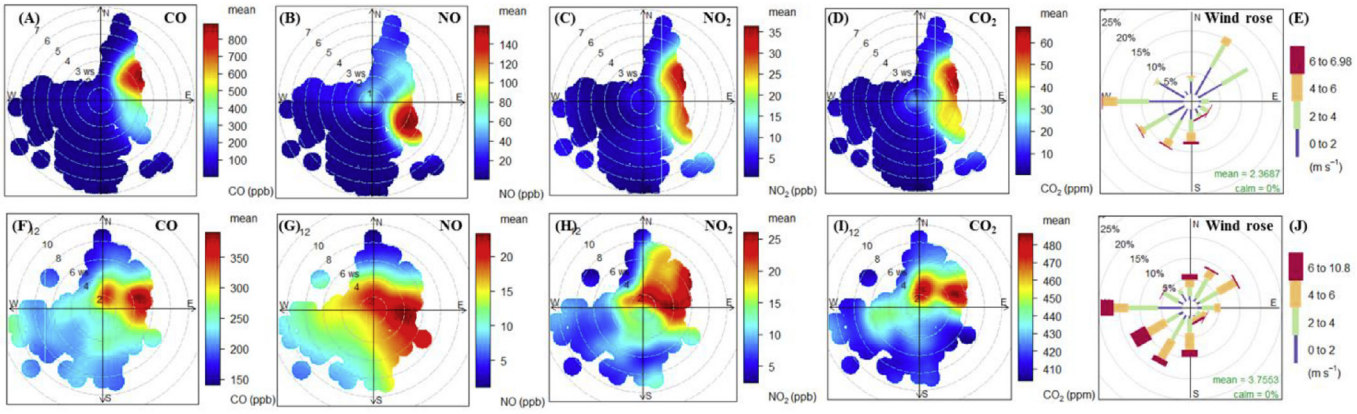

Fig. 10. Polar bivariate and wind rose plots for hourly average data at site 29 for the five-week study period. (A–E) local CO, NO, NO_2, CO_2 and wind rose, plots make use of measured wind data at site. (F–J) non-local (network baseline) CO, NO, NO_2, CO_2 and wind rose, plots make use of wind data obtained from the Met Office (Met Office, 2012) site at LHR2 and are thus representative of the large-scale flow.

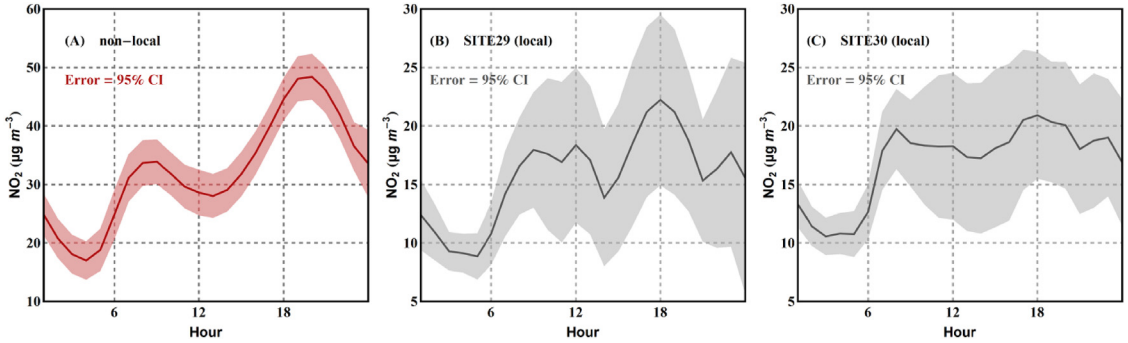

Fig. 11. Average diurnal profiles of NO_2 for the 5 week study period. (A) Non-local signature, (B) local signature at site 29 and (C) local signature at site 30. Shaded areas are 95% confidence intervals about the mean. Note NO_2 are expressed in μg m^{-3}.

Fig. 10F–I also show polar bivariate plots for CO, NO, NO_2 and CO_2, except in this case for the non-local (non-airport) component, with the meteorological measurements now taken from the Met Office site at Heathrow airport (Met Office, 2012) which can be taken to represent the large-scale wind field (Fig. 10J). Note that as these plots are derived from the entire sensor network and not from any one sensor, unlike the local site-specific signatures there is only one per species for the entire network. Firstly, we observe that, in contrast to the local pollutant signatures (Fig. 10A–D), elevated concentrations are observed at lower wind speeds when dispersion of pollutants would be expected to be reduced, but secondly there are also elevated pollutant levels when the wind is from the easterly sector, consistent with high pollutant concentrations being advected across the airport from central London (Fig. 1B).

A key feature of the non-local NO_2 signature is that its diurnal pattern (Fig. 11A), with morning and evening peaks, matches that typically seen from road traffic emissions (Vardoulakis et al., 2007). This contrasts with the diurnal profiles from the local signatures at the airport (Fig. 11B and C), which show flatter signatures during the day with a night time baseline associated with the more uniform level of daytime airport activities and the night time airport closure.

3.2. ADMS airport model and measurement comparison

This comparison uses data from the local pollution signatures extracted from the sensor network and modelled equivalent emissions for the ADMS-Airport model. The emissions and model set-up have been optimised using the sensors data, as described in section 2.4, and using known average thrust settings for British Airways (BA) aircraft at Heathrow for the period. The sensor data were averaged to hourly means to match the timescale of the ADMS-Airport model outputs. Overall, there was good agreement between the model output and the measurements for all the gas species of interest across the network, as shown in the example for site 29 close to the west end of the southern runway (Fig. 7) which compares, for each of CO, NO, NO_2 and CO_2, the local signature from the sensor with the both the refined and unrefined model prediction taking account only of the airport emissions. Both measurement (blue) and refined model (red) are consistent in showing periods of high and low daily concentrations associated different modes of runway usage as meteorological conditions vary. The peak concentrations observed in early October and the week beginning 19 October are from the southern runway under the so-called easterly runway operational mode when aircraft take-off and land into the easterly wind. Heathrow airport most frequently operates under westerly mode (take-off and landing in this direction) consistent with the prevailing wind, however if the wind is from the east, an easterly operational mode is initiated (LHR, 2017).

Fig. 12 shows a comparison of modelled and measured local NO_2 concentrations for all the active sensor sites, averaged over the five-week measurement period. Also shown are comparisons of the average

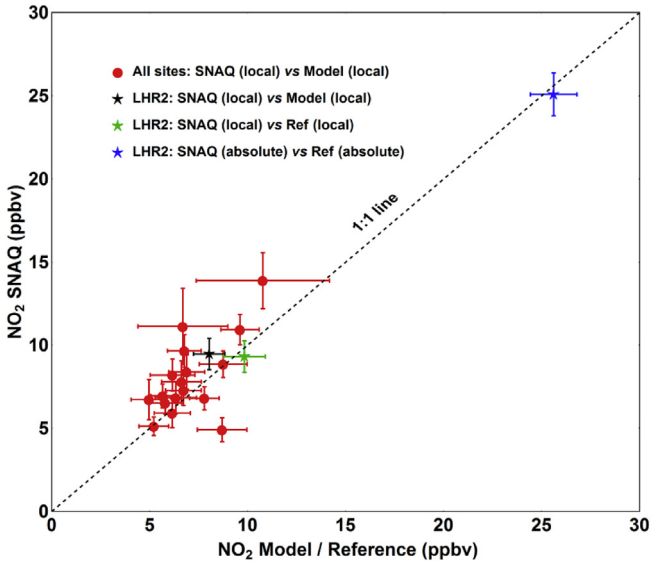

Fig. 12. Comparison of measured local NO_2 amounts for all the active sensor sites with the ADMS model averaged over the five-week measurement period (solid red circles). Also shown are the average local and total NO_2 mixing ratios at the one airport reference site (green and blue solid stars respectively) as well as the measured and modelled local NO_2 at the reference site (black). The error bars on y and x axes are ± 3σ. (For interpretation of the references to colour in this figure legend, the reader is referred to the Web version of this article.)

NO_2 local and total mixing ratios at the one reference site at the airport (LHR2). Firstly, there is broadly good correspondence between modelled and measured local NO_2 across the entire network confirming the high level of ADMS model performance. Secondly, the co-located SNAQ and reference instrument show excellent agreement both in local and absolute terms confirming the performance of the low cost NO_2 sensor.

An average absolute NO_2 concentration of 25 ppbv (~50 μg/m^3) was observed at the airport reference site (site 47), compared to local airport contribution of 9 ppbv (~18 μg/m^3). This demonstrates that local airport emissions account for only ~36% of the total NO_2 observed at that site and confirming that non-airport emissions dominate for the measurement period even at this airside location. A previous study (Carslaw et al., 2006), based on hourly NO_x and NO_2 data for 8 measurement sites in the broad neighbourhood of the airport, reported a lower bound for the airport contribution of 27%. In contrast to the current study however, in that work the background contribution was estimated from one site only so that the effect of any emission sources between that site and the airport could not be accounted for.

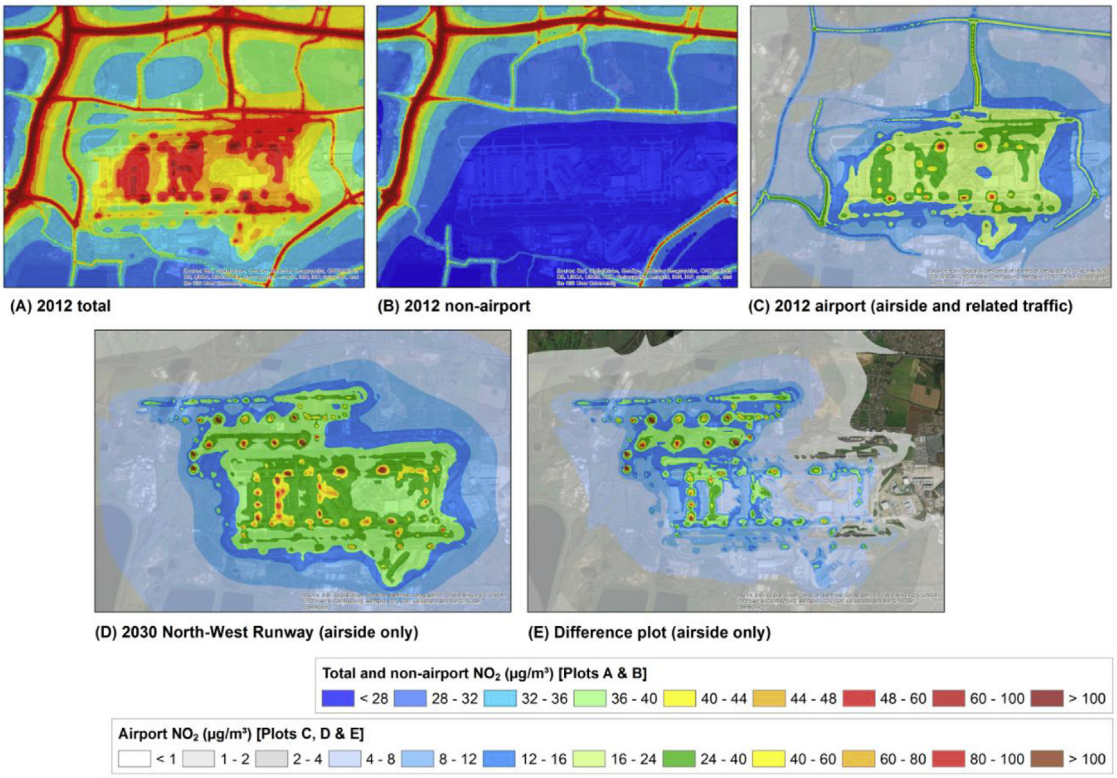

Fig. 13. Annual average modelled NO_2 concentrations (µg/m^3). (A) total NO_2 concentrations for 2012 (B) non-airport excluding airside and airport related traffic for 2012, (C) airside and airport related traffic emissions for 2012, (D) airside NO_2 concentrations for 2030 North-West Runway scenario, and (E) difference plot of the predicted contributions of the 2030 North-West Runway and 2012 baseline.

3.3. Model annual average predictions using the ADMS-Airport model

In order to identify regions where the NO_2 annual mean limit value is exceeded, we used the ADMS-Airport model, as refined by the sensor network measurements, to predict annual mean NO_2 concentration in and around Heathrow Airport. A contour plot of modelled annual average NO_2 concentrations for 2012 obtained by averaging the model output for each hour of the year is shown in Fig. 13A. This shows exceedence (yellow, orange and red) of the NO_2 limit value within and close to the airport and close to major roads. Source apportioned model calculations are depicted in Fig. 13B and C, detailing the annual average contributions of airport and non-airport emissions; the airport emissions include road traffic emissions associated with the airport.

4. Discussion and conclusion

We have used the network of sensor nodes to distinguish between and quantify local and non-local contributions to the different pollutant measurements. From this we have been able to independently derive emission ratios for the airport activities at the different node sites.

The non-airport mean NO_2 concentration contribution derived from the observations of ~16 ppbv (~32 µg/m^3) shown in Fig. 11A indicates that most of the NO_2 observed in the proximity of the airport arises from emissions which are unrelated to the airport activities. The polar bivariate plot analysis of this non-airport contribution also unequivocally indicates that the predominant non-airport emission sources are in the ENE/E direction, i.e. from the Greater London region. Importantly, the diurnal profile of this signal is characteristic of road traffic related emissions as the morning and evening rush hour peak events are clearly evident in the figure and thus it can be concluded that these sources are largely associated with road traffic emissions from Greater London.

The ADMS-Airport model, with emission indices validated and refined by comparison with the equivalent airport emissions derived directly from the sensor network measurements, shows that within the airport perimeter annual average NO_2 levels, at typically 50 µg/m^3 (Fig. 13A), are above the EU annual average limit of 40 µg/m^3. However, beyond the airport perimeter, annual average NO_2 levels only marginally exceed this limit except near major roads (40–44µg/m^3 up to 1 km to the north of the airport and lower further away). However, the model results show that in the area immediately outside the airport where the NO_2 annual average limit value is exceeded, only 12–16 µg/m^3 (~6–8 ppbv) of NO_2 (Fig. 13C) can be attributed to airport activities, ~30–36% of the total NO_2.

Model evaluations of the potential impact of an airport expansion (the addition of a third runway with its increased aircraft movements) suggest that the airport contribution to the north east of the airport will rise to ~20 µg/m^3 (~10 ppbv) with the addition of a third runway (Fig. 13D–E).

This work demonstrates a technique for source apportionment in complex environments, in this case a major international airport, using a low cost air quality sensor network. The wider impact of such work is that is can lead to an improved understanding of the impacts of policy decisions and interventions. For Heathrow airport, there is an expectation (Airports Commission July 2015) that on the timescale of the airport expansion, changes to the road traffic fleet, particularly the introduction of cleaner (Euro 6) and zero emission vehicles, NOx levels in the London plume reaching the airport will fall significantly. As an example of the likely magnitude of this effect, projections from 2013 to 2030 using the Emission Factor Toolkit (EFT) 7 published by Defra (2016) suggest a reduction of more than 80% in road NO_x emissions just to the north of the airport (see section 2.4.4). If this projection is correct, then even with a third runway and the associated roadside activities, NO_2 levels would be expected to fall below the current NO_2 annual average limit, meaning that the area would then be compliant for NO_2. Clearly crucial to achieving compliance with the NO_2 annual

average limit value by 2030 would be the extent to which vehicle engine technologies do indeed reduce NO_x emissions across the vehicle fleet.

The critical components of this study are the explicit separation of local and non-local emissions and the direct determination of emission indices using the sensor network coupled to appropriate analysis methods, and together are important demonstrations of the potential of this emerging low-cost air quality sensor technology.

Heathrow airport represents in some senses a special case, particularly in that on the spatial scale of the airport the pollutant baselines at any time can be represented by single values. Extending the technique across wider domains such as across an entire mega-city, while conceptually very similar to the approach we have taken, would be expected to require baselines which could vary spatially.

The measurement and analysis methodology we have demonstrated in this case study has wide applicability in many complex air quality environments including developing megacities, and has the clear potential to inform in a cost-effective manner policies and interventions which would mitigate potential health impacts of air quality and other environmental issues including the monitoring of greenhouse gas emissions.

Acknowledgment

The authors would like to thank NERC, United Kingdom NE/I007490/1 for funding the SNAQ London Heathrow project. We would also like to acknowledge David Vowles, Spencer Thomas and Luke Cox of Heathrow Airport Limited for helping with the logistics at Heathrow Airport.

Appendix A. Supplementary data

Supplementary data to this article can be found online at https://doi.org/10.1016/j.atmosenv.2018.09.030.

References

AEA, Energy & Environment, 2010. Heathrow airport emission inventory 2008/9, AEAT/ENV/R/2906 issue 2. Document 04 app H emissions inventory in background information volume 1 submitted by heathrow airports limited to the airports commission. https://www.gov.uk/government/uploads/system/uploads/attachment_data/file/368785/reports-04to39.zip.

Air Quality Studies for Heathrow, 2007. Base Case, Segregated Mode, Mixed Mode and Third Runway Scenarios Modelled Using ADMS-airport, Cambridge Environmental Research Consultants. Report Ref FM699/R23_Final/07. http://cerc.co.uk/environmental-software/assets/data/doc_validation/ADMS-Airport_Adding%20Capacity_Air%20Quality.pdf.

Airports Commission July, 2015. Airports Commission: Final Report. ISBN: 978-1-84864-158-7. https://www.gov.uk/government/uploads/system/uploads/attachment_data/file/440316/airports-commission-final-report.pdf.

Bennett, M., Christie, S., Graham, A., Raper, D., 2010. Lidar observations of aircraft exhaust plumes. J. Atmos. Ocean. Technol. 27, 1638–1651. https://doi.org/10.1175/2010jtecha1412.1.

Bernstein, J.A., Alexis, N., Barnes, C., Bernstein, I.L., Nel, A., Peden, D., Diaz-Sanchez, D., Tarlo, S.M., Williams, P.B., 2004. Health effects of air pollution. J. Allergy Clin. Immunol. 114, 1116–1123. https://doi.org/10.1016/j.jaci.2004.08.030.

Borrego, C., Costa, A.M., Ginja, J., Amorim, M., Coutinho, M., Karatzas, K., Sioumis, T., Katsifarakis, N., Konstantinidis, K., De Vito, S., Esposito, E., Smith, P., André, N., Gérard, P., Francis, L.A., Castell, N., Schneider, P., Viana, M., Minguillón, M.C., Reimringer, W., Otjes, R.P., von Sicard, O., Pohle, R., Elen, B., Suriano, D., Pfister, V., Prato, M., Dipinto, S., Penza, M., 2016. Assessment of air quality microsensors versus reference methods: the EuNetAir joint exercise. Atmos. Environ. 147, 246–263. https://doi.org/10.1016/j.atmosenv.2016.09.050.

Brunekreef, B., Holgate, S., 2002. Air pollution and health. Lancet 360, 1233–1242. https://doi.org/10.1016/s0140-6736(02)11274-8.

Carslaw, D.C., Beevers, S.D., Ropkins, K., Bell, M.C., 2006. Detecting and quantifying aircraft and other on-airport contributions to ambient nitrogen oxides in the vicinity of a large international airport. Atmos. Environ. 40, 5424–5434. https://doi.org/10.1016/j.atmosenv.2006.04.062.

Carslaw, D.C., Ropkins, K., 2012. Openair — an R package for air quality data analysis. Environ. Model. Software 27–28, 52–61. https://doi.org/10.1016/j.envsoft.2011.09.008.

Crilley, L.R., Shaw, M., Pound, R., Kramer, L.J., Price, R., Young, S., Lewis, A.C., Pope, F.D., 2018. Evaluation of a low-cost optical particle counter (Alphasense OPC-N2) for ambient air monitoring. Atmos. Meas. Tech. Discuss. 11, 709–720. https://doi.org/10.5194/amt-11-709-2018.

Defra, 2016. UK department for environment Food and rural Affairs, emission factor Toolkit v7.0. https://laqm.defra.gov.uk/review-and-assessment/tools/emissions-factors-toolkit.html.

Department for Environment, Food and Rural Affairs, 2016. Local air quality management, NO_X to NO_2 calculator. https://laqm.defra.gov.uk/review-and-assessment/tools/background-maps.html#NOxNO2calc.

De Vito, S., Esposito, E., Salvato, M., Popoola, O., Formisano, F., Jones, R., Di Francia, G., 2018. Calibrating chemical multisensory devices for real world applications: an in-depth comparison of quantitative machine learning approaches. Sensor. Actuator. B Chem. 255, 1191–1210. https://doi.org/10.1016/j.snb.2017.07.155.

Doc 9889, 2011. Airport Air Quality Manual. International Civil Aviation Organization ISBN 978-92-9231-862-8.

European Civil Aviation Conference, 2005. Report on Standard Method of Computing Noise Contours Around Civil Airports. third ed. ECAC Document 29.

Heimann, I., Bright, V.B., McLeod, M.W., Mead, M.I., Popoola, O.A.M., Stewart, G.B., Jones, R.L., 2015. Source attribution of air pollution by spatial scale separation using high spatial density networks of low cost air quality sensors. Atmos. Environ. 113, 10–19. https://doi.org/10.1016/j.atmosenv.2015.04.057.

Herndon, S.C., Jayne, J.T., Lobo, P., Onasch, T.B., Fleming, G., Hagen, D.E., Whitefield, P.D., Miake-Lye, R.C., 2008. Commercial aircraft engine emissions characterization of in-use aircraft at hartsfield-jackson atlanta international airport. ES T (Environ. Sci. Technol.) 42, 1877–1883. https://doi.org/10.1021/es072029+.

Herndon, S.C., Shorter, J.H., Zahniser, M.S., Nelson, D.D., Jayne, J., Brown, R.C., Miake-Lye, R.C., Waitz, I., Silva, P., Lanni, T., Demerjian, K., Kolb, C.E., 2004. NO and NO2 emission ratios measured from in-use commercial aircraft during taxi and takeoff. ES T (Environ. Sci. Technol.) 38, 6078–6084. https://doi.org/10.1021/es049701c.

Hu, S., Fruin, S., Kozawa, K., Mara, S., Winer, A.M., Paulson, S.E., 2009. Aircraft emission impacts in a neighborhood adjacent to a general aviation airport in southern California. ES T (Environ. Sci. Technol.) 43, 8039–8045. https://doi.org/10.1021/es900975f.

Independent report, 2014. Additional Airport Capacity: Heathrow Airport North West Runway. Heathrow Airports Limited.

Jenkin, M.E., 2004. Analysis of sources and partitioning of oxidant in the UK—Part 1: the NO_X-dependence of annual mean concentrations of nitrogen dioxide and ozone. Atmos. Environ. 38, 5117–5129. https://doi.org/10.1016/j.atmosenv.2004.05.056.

Kim, J., Shusterman, A.A., Lieschke, K.J., Newman, C., Cohen, R.C., 2018. The BErkeley atmospheric CO2 observation network: field calibration and evaluation of low-cost air quality sensors. Atmos. Meas. Tech. Discuss. 11, 1937–1946. https://doi.org/10.5194/amt-11-1937-2018.

Kumar, P., Morawska, L., Martani, C., Biskos, G., Neophytou, M., Di Sabatino, S., Bell, M., Norford, L., Britter, R., 2015. The rise of low-cost sensing for managing air pollution in cities. Environ. Int. 75, 199–205. https://doi.org/10.1016/j.envint.2014.11.019.

Lewis, A.C., Lee, J.D., Edwards, P.M., Shaw, M.D., Evans, M.J., Moller, S.J., Smith, K.R., Buckley, J.W., Ellis, M., Gillot, S.R., White, A., 2016. Evaluating the performance of low cost chemical sensors for air pollution research. Faraday Discuss 189, 85–103. https://doi.org/10.1039/c5fd00201j.

LHR Airport Limited. http://www.heathrow.com/noise/heathrow-operations/cranford-agreement#, Accessed date: 3 November 2016.

LHR, 2017. Heathrow Operations: Wind Direction. LHR Airports Limited. http://www.heathrow.com/noise/heathrow-operations/wind-direction.

Lowry, D., Lanoisellé, M.E., Fisher, R.E., Martin, M., Fowler, C.M.R., France, J.L., Hernández-Paniagua, I.Y., Novelli, P.C., Sriskantharajah, S., O'Brien, P., Rata, N.D., Holmes, C.W., Fleming, Z.L., Clemitshaw, K.C., Zazzeri, G., Pommier, M., McLinden, C.A., Nisbet, E.G., 2016. Marked long-term decline in ambient CO mixing ratio in SE England, 1997–2014: evidence of policy success in improving air quality. Sci. Rep. 6, 25661. https://doi.org/10.1038/srep25661.

Masiol, M., Harrison, R.M., 2015. Quantification of air quality impacts of London heathrow airport (UK) from 2005 to 2012. Atmos. Environ. 116, 308–319. https://doi.org/10.1016/j.atmosenv.2015.06.048.

McConnell, R., Berhane, K., Gilliland, F., London, S.J., Islam, T., Gauderman, W.J., Avol, E., Margolis, H.G., Peters, J.M., 2002. Asthma in exercising children exposed to ozone: a cohort study. Lancet 359, 386–391. https://doi.org/10.1016/S0140-6736(02)07597-9.

McHugh, C.A., Carruthers, D.J., Edmunds, H.A., 1997. ADMS–Urban: an air quality management system for traffic, domestic and industrial pollution. Int. J. Environ. Pollut. 8, 666–674. https://doi.org/10.1504/ijep.1997.028218.

Mead, M.I., Popoola, O.A.M., Stewart, G.B., Landshoff, P., Calleja, M., Hayes, M., Baldovi, J.J., McLeod, M.W., Hodgson, T.F., Dicks, J., Lewis, A., Cohen, J., Baron, R., Saffell, J.R., Jones, R.L., 2013. The use of electrochemical sensors for monitoring urban air quality in low-cost, high-density networks. Atmos. Environ. 70, 186–203. https://doi.org/10.1016/j.atmosenv.2012.11.060.

Met Office, 2012. Met Office Integrated Data Archive System (MIDAS) Land and Marine Surface Stations Data (1853-current). NCAS British Atmospheric Data Centre [cited: 6 August, 2013].

Miskell, G., Salmond, J., Williams, D.E., 2017. Low-cost sensors and crowd-sourced data: observations of siting impacts on a network of air-quality instruments. Sci. Total Environ. 575, 1119–1129. https://doi.org/10.1016/j.scitotenv.2016.09.177.

Module 6, 2015. Air Quality Local Assessment Detailed Emissions Inventory and Dispersion Modelling. Jacobs UK Limited.

Mueller, M., Meyer, J., Hueglin, C., 2017. Design of an ozone and nitrogen dioxide sensor unit and its long-term operation within a sensor network in the city of Zurich. Atmos. Meas. Tech. 10, 3783–3799. https://doi.org/10.5194/amt-10-3783-2017.

National Audit Office, 2009. Air quality, briefing for the house of commons environmental Audit committtee. https://www.nao.org.uk/wp-content/uploads/2010/01/

Air_Quality.pdf.
Parnia, S., Brown, J.L., Frew, A.J., 2002. The role of pollutants in allergic sensitization and the development of asthma. Allergy 57, 1111–1117. https://doi.org/10.1034/j.1398-9995.2002.02167.x.
Penza, M., Suriano, D., Villani, M.G., Spinelle, L., Gerboles, M., 2014. Towards air quality indices in smart cities by calibrated low-cost sensors applied to networks. In: IEEE SENSORS 2014 Proceedings, pp. 2012–2017. https://doi.org/10.1109/icsens.2014.6985429.
Pope, C.A., Dockery, D.W., 2006. Health effects of fine particulate air pollution: lines that connect. J Air Waste Manage 56, 709–742. https://doi.org/10.1080/10473289.2006.10464485.
Popoola, O., Mead, I., Bright, V., Baron, B., Saffell, J., Stewart, G., Kaye, P., Jones, R., 2013. A portable low-cost high density sensor network for air quality at London Heathrow airport. In: AGU 2013 Fall Meeting, San Francisco, California.
Popoola, O.A.M., Stewart, G.B., Mead, M.I., Jones, R.L., 2016. Development of a baseline-temperature correction methodology for electrochemical sensors and its implications for long-term stability. Atmos. Environ. 147, 330–343. https://doi.org/10.1016/j.atmosenv.2016.10.024.
Ren, M., Li, N., Wang, Z., Liu, Y., Chen, X., Chu, Y., Li, X., Zhu, Z., Tian, L., Xiang, H., 2017. The short-term effects of air pollutants on respiratory disease mortality in Wuhan, China: comparison of time-series and case-crossover analyses. Sci. Rep. 7, 40482. https://doi.org/10.1038/srep40482.
Samoli, E., Peng, R., Ramsay, T., Pipikou, M., Touloumi, G., Dominici, F., Burnett, R., Cohen, A., Krewski, D., Samet, J., Katsouyanni, K., 2008. Acute effects of ambient particulate matter on mortality in europe and north America: results from the APHENA study. Environ. Health Perspect. 116, 1480–1486. https://doi.org/10.1289/ehp.11345.
Schneider, P., Castell, N., Vogt, M., Dauge, F.R., Lahoz, W.A., Bartonova, A., 2017. Mapping urban air quality in near real-time using observations from low-cost sensors and model information. Environ. Int. 106, 234–247. https://doi.org/10.1016/j.envint.2017.05.005.
Schürmann, G., Schäfer, K., Jahn, C., Hoffmann, H., Bauerfeind, M., Fleuti, E., Rappenglück, B., 2007. The impact of NOx, CO and VOC emissions on the air quality of Zurich airport. Atmos. Environ. 41, 103–118. https://doi.org/10.1016/j.atmosenv.2006.07.030.
Spinelle, L., Gerboles, M., Villani, M.G., Aleixandre, M., Bonavitacola, F., 2015. Field calibration of a cluster of low-cost available sensors for air quality monitoring. Part A: ozone and nitrogen dioxide. Sensor. Actuator. B Chem. 215, 249–257. https://doi.org/10.1016/j.snb.2015.03.031.
Sun, L., Westerdahl, D., Ning, Z., 2017. Development and evaluation of A novel and cost-effective approach for low-cost NO(2) sensor drift correction. Sensors 17, 1916. https://doi.org/10.3390/s17081916.
Sun, L., Wong, K.C., Wei, P., Ye, S., Huang, H., Yang, F., Westerdahl, D., Louie, P.K.K., Luk, C.W.Y., Ning, Z., 2016. Development and application of a next generation air sensor network for the Hong Kong marathon 2015 air quality monitoring. Sensors 16, 211. https://doi.org/10.3390/s16020211.
Updated Air Quality Re-analysis, 2017. Impact of New Copert Emission Factors and Associated New Pollution Climate Mapping Sensitivity Testing. WSP Parsons Brinckerhoff Report No. 62103867-041. https://www.gov.uk/government/uploads/system/uploads/attachment_data/file/588752/updated-air-quality-re-analysis.pdf.
UK Department for Transport, 2006. Project for the Sustainable Development of Heathrow – Report of the Air Quality Technical Panel Chapter 4 – Dispersion Modelling. . http://webarchive.nationalarchives.gov.uk/20071209143920/http://www.dft.gov.uk/pgr/aviation/environmentalissues/heathrowsustain/chapter4dispersionmodelling.
UK Department for Transport, 2017. Consultation on Draft Airports National Policy Statement: New Runway Capacity and Infrastructure at Airports in the South East of England. ISBN:978-1-84864-189-1. https://www.gov.uk/government/uploads/system/uploads/attachment_data/file/589082/consultation-on-draft-airports-nps.pdf.
Vardoulakis, S., Valiantis, M., Milner, J., ApSimon, H., 2007. Operational air pollution modelling in the UK—street canyon applications and challenges. Atmos. Environ. 41, 4622–4637. https://doi.org/10.1016/j.atmosenv.2007.03.039.
Venkatram, A., Karamchandani, P., Pai, P., Goldstein, R., 1994. The development and application of a simplified ozone modeling system (SOMS). Atmos. Environ. 28, 3665–3678. https://doi.org/10.1016/1352-2310(94)00190-V.
WHO, 2009. Ambient air pollution: a global assessment of exposure and burden of disease, geneva. http://apps.who.int/iris/bitstream/10665/250141/1/9789241511353-eng.pdf.